Supporting Information

Fully Inkjet-printed PEDOT:PSS/NiO/Colloidal $CsPbBr_3/SnO_2$ Perovskite LED on Rigid and Flexible Substrates

Giovanni Vescio, Gayathri Mathiazhagan, * Sergio González-Torres, Jesús Sanchez-Diaz, Alexis Villanueva-Antoli, Rafael S. Sánchez, Andrés F. Gualdrón-Reyes, Marek Oszajca, Flavio Linardi , Alina Hauser, Sergi Hernández, Iván Mora-Seró, * Albert Cirera, Blas Garrido.*

Table S1. Partially and one fully inkjet-printed perovskite based LEDs.

Year	Structure	Layers inkjet printed	Peak emission (nm)	Max Luminance (cd/m2)	Max Current Efficiency (cd/A)	Max. EQE (%)	Luminance decay	Ref.
2020	ITO/PEDOT:PSS/PVK/Poly-TPD/$FA_{0.3}Cs_{0.7}PbBr$/TPBi/LiF/Al	$FA_{0.3}Cs_{0.7}PbBr$	520	1233	10.3	2.8	7 min 90cd/m²→45cd/m² (-50% in 7 min)	[1]
2020	ITO/PEDOT:PSS/ /$MAPbBr_3$/BCP/LiF/Al	$MAPbBr_3$	530	4000	≈0.9	N.A.	N.A.	[2]
2021	ITO/PEDOT:PSS/TFB /$CsPbBr_3$/TPBi/LiF/Al	$CsPbBr_3$	515	10992	8.67	3.03	N.A.	[3]
2021	ITO/TFB /PVK/$PEA_2Cs_{n-1}PbnBr_{3n+1}$ /TPBi/LiF/Al	$PEA_2Cs_{n-1}PbnBr_{3n+1}$	530	3640	31.5	9.0	10 min 120cd/m²→50cd/m² (-42% in 10 min)	[4]
2021	PEDOT:PSS/ $MAPbBr_3$/PEI/AgNWs	*All inkjet printed*	536	10227	2.01	0.8	-10% in 100h	[5]
2022	PEDOT:PSS/PTAA/Perovskite /TPBi/ LiF/Al	$CsPbBr_3$ $CsPbI_3$ $CsPbBrxCl_{1-x}$	517 688 488	43883	31.15	8.54 5.54 0.81	-50% in 64 min -50% in 34 min -50% in 2 min	[6]
2022	PEDOT:PSS/MoO_3/PVK/$FAPb_{0.7}Sn_{0.3}Br_3$ /TPBi/ LiF/Al	$FAPb_{0.7}Sn_{0.3}Br_3$	≈520	2465	32	7.9	45 s 2000cd/m²→100cd/m² (-50% in 5s)	[7]
2022	ITO/PEDOT:PSS/ PEA_2SnI_4 /PO-T2T/LiF/Al	PEA_2SnI_4	633	30	0.5	1	N.A.	[8]
2022	ITO/PEDOT:PSS/$MAPbCl_3$ /mCP:Ir(mppy)3/TPBi/Liq/Al	PEDOT:PSS/$MAPbCl_3$ /mCP:Ir(mppy)3	510	5038	30.8	8.9	N.A.	[9]
2022	ITO/Poly-TPD/PFN-Br/$CsPbBr_3$+$PEAPbBr_3$ /LiF/TPBi/LiF/Al	$CsPbBr_3$+$PEAPbBr_3$	512	12882	29.4	10.1	-50% in 35 min	[10]
2023	ITO/PEDOT:PSS/ /$MAPbBr_3$+PEG/BCP or TPBi/LiF/Al	$MAPbBr_3$ +PEG	530	3598	2.6	N.A.	N.A.	[11]

Results of p-n junctions:

Subsequent to the evaluation of stand-alone IJP NiO thin films, their printability was checked on PEDOT layer. Very low contact angles of $\theta < 25^{o}$ (see Figure S1a) was observed allowing for the maximum control of layer thickness by drop spacing parameter (drop-per-inch around 360, drop distance 70 µm). Thus, visibly smooth NiO layer can be inkjet-printed on PEDOT (Figure S1b in the supplementary information).

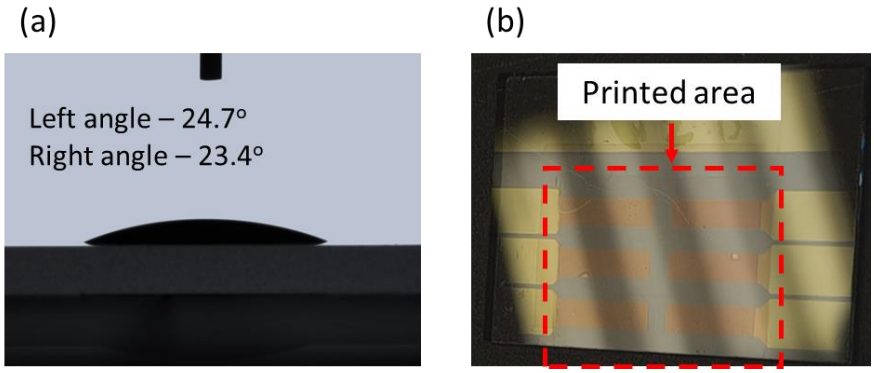

Figure S1: (a) Contact angle measurement of IJP NiO on PEDOT. (b) Picture of IJP NiO on ITO/SC PEDOT showing smooth, homogeneous and pin-hole free layer.

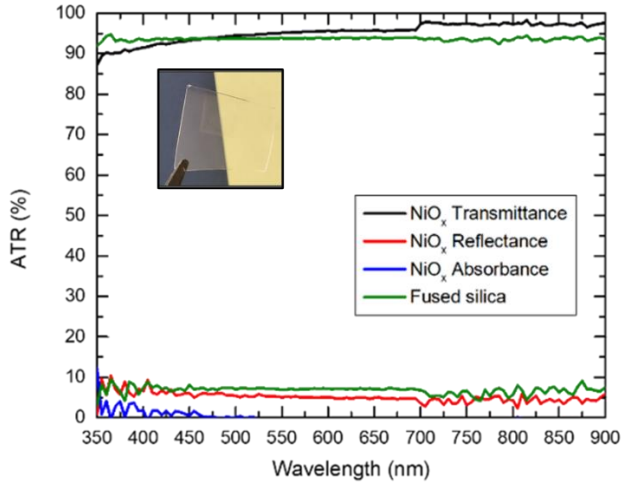

Figure S2: UV-Vis spectroscopy measurements of IJP NiO on fused silica. Greater than 90% transmittance in the visible region indicates a transparent IJP NiO layer. Inset shows the image of transparent IJP NiO film on fused silica.

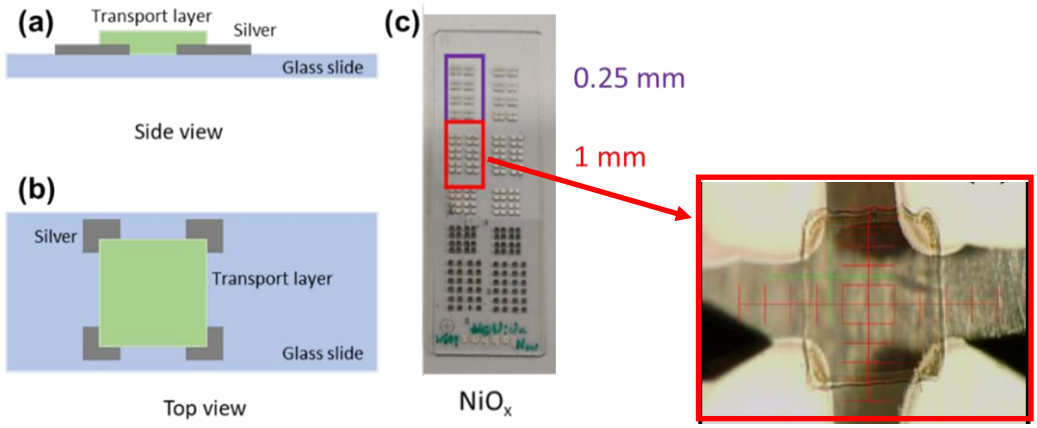

Figure S3: Setup for conductivity measurements through Van der Pauw 4-probe method. (a) Cross-sectional view of how the IJP transport layer is connected to the electrode is shown. (b) Top view of the inkjet-printed layer and its connection to the electrodes. (c) Different sizes of the IJP NiO_X square on a glass substrate. Marked in violet and red is the length of the square.

In order to ensure the expected electrical characteristics of the inkjet-printed charge injection layers, several p-n junctions were fabricated. Following we present three different p-n structures which were fabricated where the HIL/HTM was either spin-coated (SC) or inkjet-printed (IJP) or the combination of both. In all conditions, 2,4,6-tris[3(diphenylphosphinyl)phenyl]-1,3,5-triazine (POT2T) was selected as ETM which was always evaporated (details under Device fabrication section):

- **p-n structure_1**: SC PEDOT/Evaporated POT2T,
- **p-n structure_2**: SC PEDOT/ IJP NiO_X/Evaporated POT2T,
- **p-n structure_3**: IJP PEDOT/ IJP NiO_X/Evaporated POT2T.

Their electrical characterization results are demonstrated in Figure S4. The inset of the figure presents the details of the average current values measured for more than 30 devices under positive bias (8 V). Different box plots corresponding to the maximum currents of the three p-n structures, confirm that the inkjet-printed HIL/HTM stack (p-n structure_3) showed the same electrical behaviour as the single SC PEDOT layer (p-n structure_1). Their average current values were in the range of few 10 mA. Contrarily, for the p-n junctions where a dual layer HIL/HTM stack is fabricated consisting of SC PEDOT/IJP NiO_X (p-n structure_2), the average current values decreased by more than one order of magnitude. The complete electrical curve of each structure shows that there is an increase of series resistance for the dual layer HIL/HTM stack (p-n structure_2) configuration. It is reflected as a lower performance in terms of maximum current and turn on voltage value (around 4 V). This can be attributed to the bad interface between spin-coated PEDOT:PSS and inkjet-printed NiO_X. Whereas, the other two configurations (p-n structure_1 and p-n structure_3), at forward biased condition, present a turn on voltage already at 3 V. This behaviour was observed for multiple devices of p-n structures mentioned above. The exponential tendencies of characteristic I-V curves after the turn on voltage for the best performing p-n devices demonstrate a favourable rectification behaviour with low leakage current. Therefore, the resulting non-linear I-V curves points to the absence of ohmic shunts confirming that all the inkjet-printed thin films are uniform and homogeneous pinhole free layers.

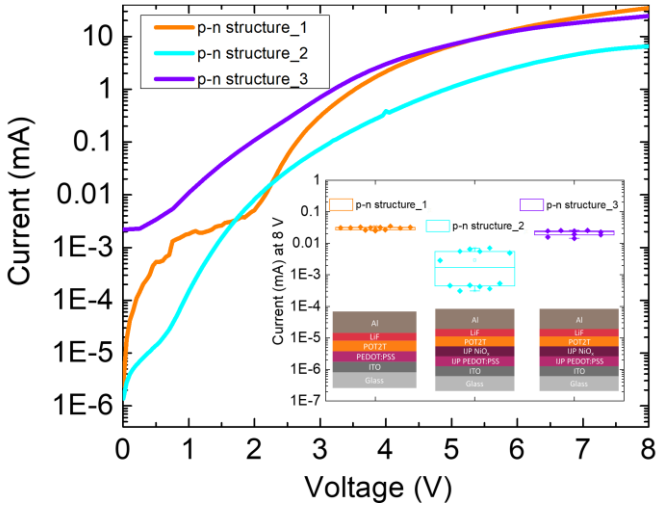

Figure S4: Results of different p-n junctions (inset) Box plots of average current values taken at 8 V. Comparing I-V curves of different p-n junctions analysed in linear scale. Active area is 0.045 cm^2.

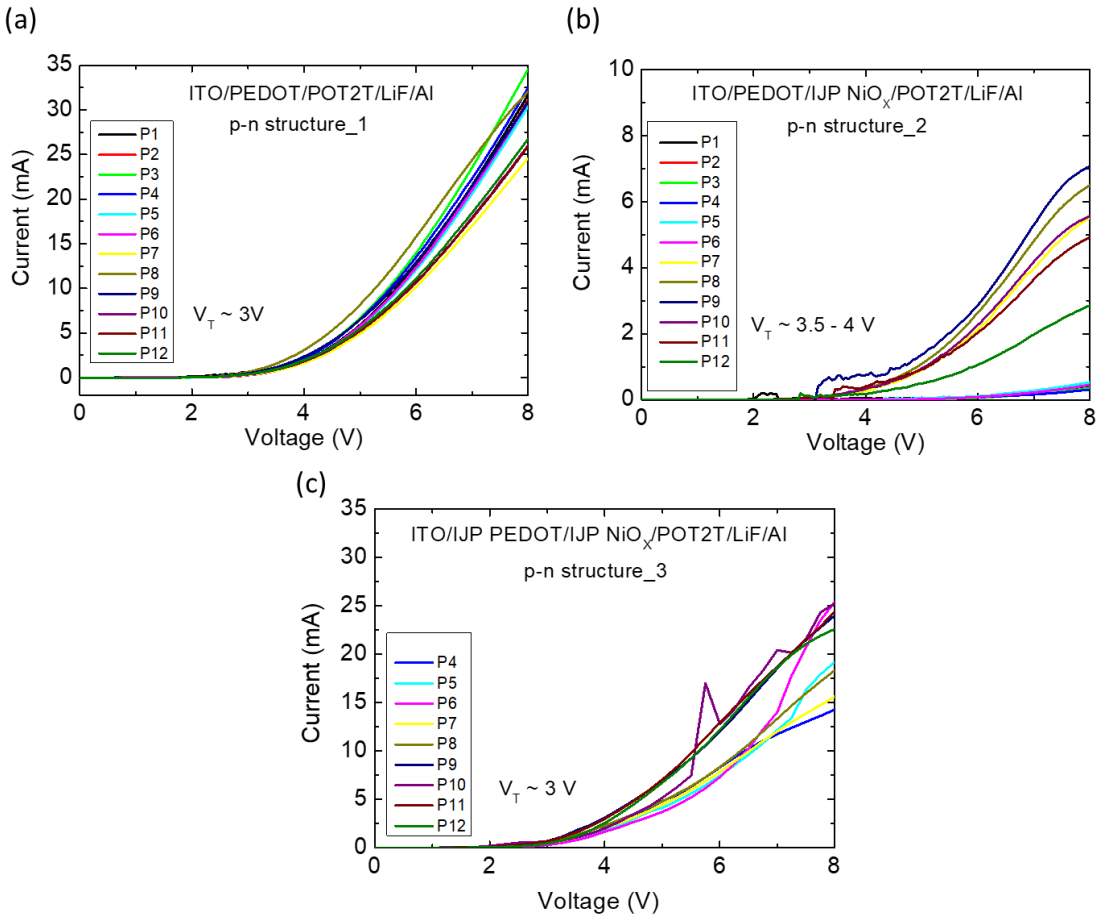

Figure S5: I-V curves in linear scale for all p-n junctions (a) p-n structure_1 (b) p-n structure_2 and (c) p-n structure_3. All these devices have POT2T as EIL. Active area is 0.045 cm^2. Turn on voltage is seen around 3 V or 4 V with a good rectification behaviour.

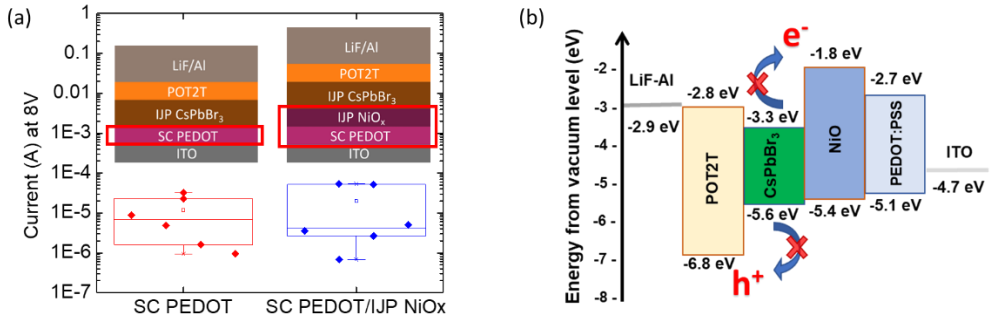

Figure S6: Results of complete PeLEDs with and without IJP NiO whose PEDOT:PSS was spin-coated. (a) Box plots of average current values taken at 8 V. Corresponding device architectures are shown in the inset. (b) Energy band diagram for the proposed architecture.[12–16]

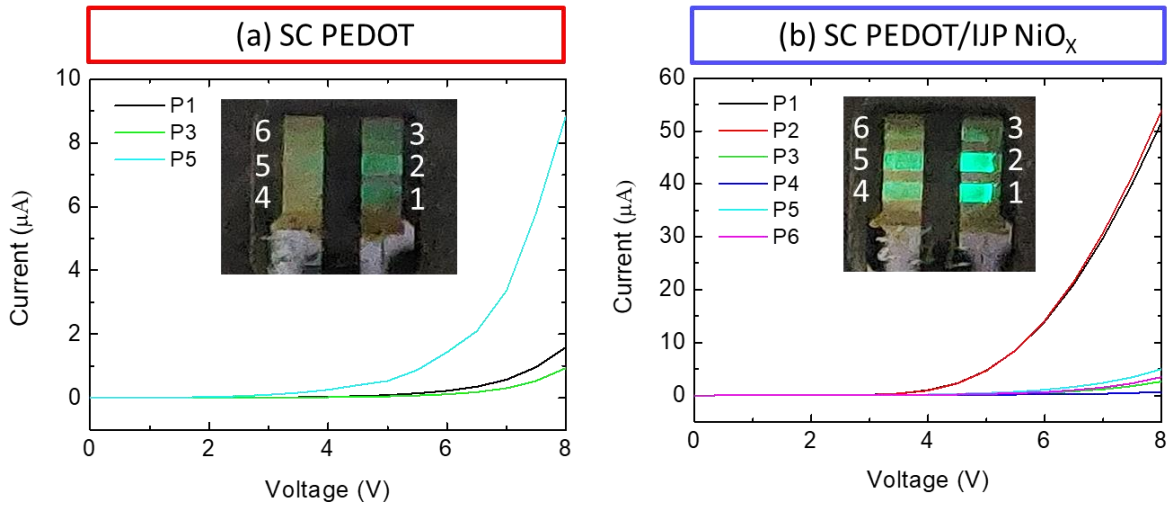

Figure S7: I-V curves in linear scale for all complete PeLEDs. (a) SC PEDOT (b) with SC PEDOT/IJP NiO_X. Active area is 0.045 cm^2. Inset shows the image of the emission of all devices in a substrate at a bias voltage of 8 V.

Comparision of PeLEDs with IJP NiO and spin-coated Poly TPD:

Poly TPD is one of the popularly used HTM/EBL layer to overcome hole injection barrier[17] and induce faster hole mobility (~ 1 x 10^{-6} cm^2 V^{-1} s^{-1}).[18] Its CB and VB levels are at -5.3 eV and 2.4 eV respectively.[19] These values are comparable with energy band levels of IJP NiO except the latter presents a favourable higher VB at -1.8 eV. For these reasons, the performance of PeLEDs with IJP NiO as EBL is compared with spin-coated Poly TPD. They conduct similar currents, and both devices show similar current density, luminance and EQE values until 6.5 V as seen in Figure S8a,b,c respectively. All values used are average values with standard deviation values of 8 devices present in two substrate with an active area of 0.08 cm^2. EL spectrum of both devices shown in Figure S8d attributes to the characteristic emission wavelength of $CsPbBr_3$ at 522 nm with high purity (FWHM = 21 nm). Subsequently, a high luminance of 17920 cd/m^2 and EQE of 2.6% was achieved for both PeLEDs structure confirming the feseability of PeLEDs with architecture ITO/SC PEDOT/IJP NiO/IJP $CsPbBr_3$/POT2T/ LiF/ Al.

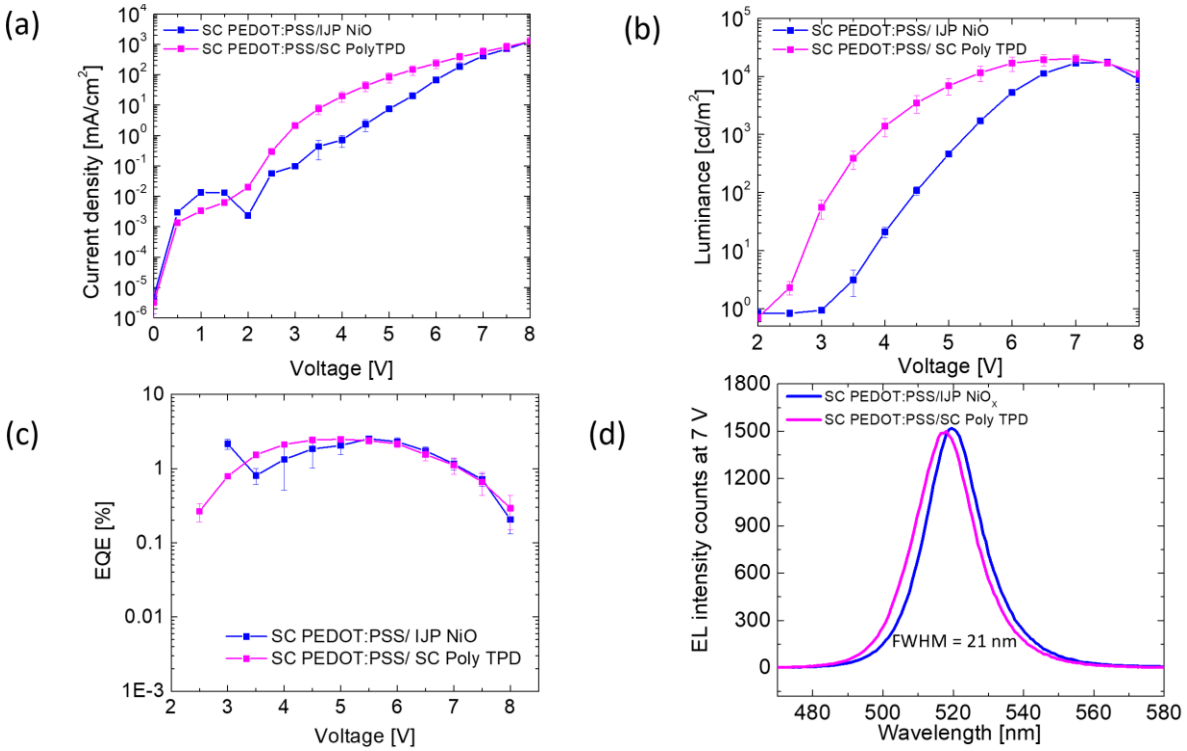

Figure S8: Results comparing PeLEDs with IJP NiO_X and spin-coated Poly TPD as EBL. (a) I-V curves. (b) L-V curves. (c) EQE with respect to voltage. The individual points in the curves of (a), (b) and (c) corresponds to average values of 4 devices with an active area of 0.08 cm^2. (d) Normalized EL intensity of the emitted wavelength at a bias voltage of 7 V. Peak counts at 522 nm corresponds to the characteristic green colour of $CsPbBr_3$.

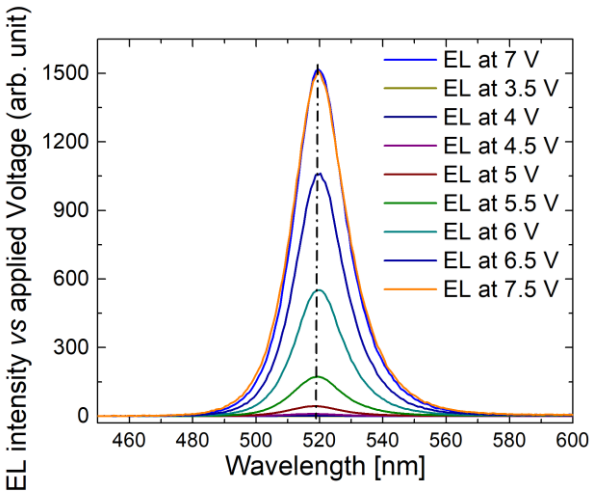

Figure S9: EL emission spectrum showing the peak emission at 520 nm (blue line) with a narrow FWMH of ~ 22 nm as function of the applied voltages.

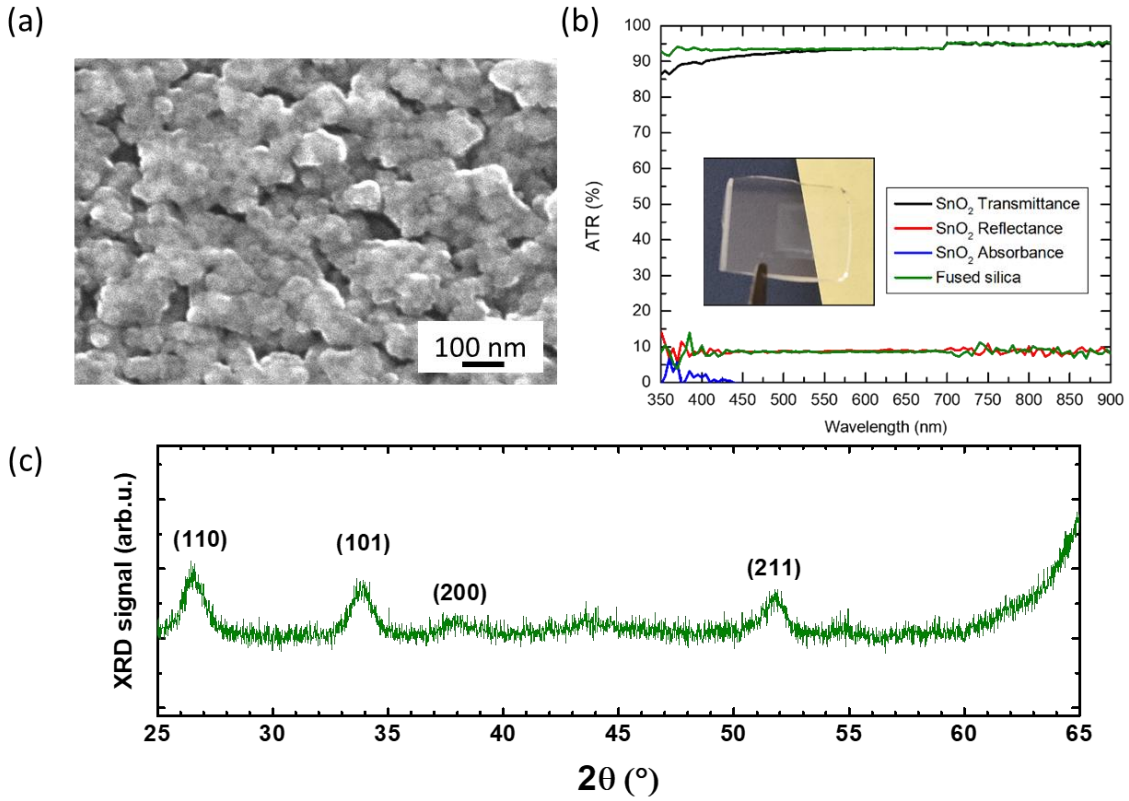

Figure S10: Results of stand-alone IJP SnO_2 layers. (a) Top view SEM image. (b) UV-Vis spectroscopy measurements of IJP SnO_2 on fused silica. Greater than 90% transmittance in the visible region indicates a transparent IJP SnO_2 layer. Inset shows the image of transparent IJP SnO_2 film on fused silica. (c) XRD pattern on IJP SnO_2 showing characteristic peaks relating to tetragonal phase of SnO_2 at 2θ of 26.7° (110), 33.97° (101), 38° (200), and 54.8° (211).

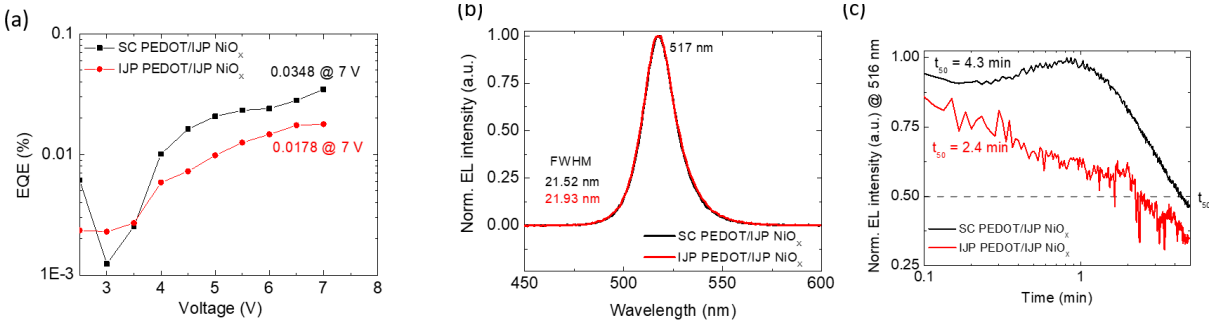

Figure S11: Results of PeLEDs with IJP SnO_2 as EIL. Comparison of devices having SC PEDOT and IJP PEDOT is shown. (a) EQE vs Voltage curve characteristics. (b) Normalised EL emission spectrum showing the peak emission at 517 nm with a narrow FWMH of ~ 22 nm. (c) Stability measurement monitoring the luminance value over time where the initial luminance was set as 100 cd/m^2. The active area of the devices is 0.08 cm^2.

Bibliography

[1] D. Li, J. Wang, M. Li, G. Xie, B. Guo, L. Mu, H. Li, J. Wang, H. L. Yip, J. Peng, *Adv Mater Technol* **2020**, *5*, DOI 10.1002/admt.202000099.

[2] F. Hermerschmidt, F. Mathies, V. R. F. Schröder, C. Rehermann, N. Z. Morales, E. L. Unger, E. J. W. List-Kratochvil, *Mater Horiz* **2020**, *7*, 1773.

[3] C. Zheng, X. Zheng, C. Feng, S. Ju, Z. Xu, Y. Ye, T. Guo, F. Li, *Org Electron* **2021**, *93*, DOI 10.1016/j.orgel.2021.106168.

[4] Y. Li, Z. Chen, D. Liang, J. Zang, Z. Song, L. Cai, Y. Zou, X. Wang, Y. Wang, P. Li, X. Gao, Z. Ma, X. Mu, A. El-Shaer, L. Xie, W. Su, T. Song, B. Sun, *Adv Opt Mater* **2021**, *9*, DOI 10.1002/adom.202100553.

[5] J. Zhao, L. W. Lo, H. Wan, P. Mao, Z. Yu, C. Wang, *Advanced Materials* **2021**, *33*, DOI 10.1002/adma.202102095.

[6] C. Wei, W. Su, J. Li, B. Xu, Q. Shan, Y. Wu, F. Zhang, M. Luo, H. Xiang, Z. Cui, H. Zeng, *Advanced Materials* **2022**, *34*, DOI 10.1002/adma.202107798.

[7] T. Ye, S. Jia, Z. Wang, R. Cai, H. Yang, F. Zhao, Y. Tan, X. Sun, D. Wu, K. Wang, *Micromachines (Basel)* **2022**, *13*, DOI 10.3390/mi13070983.

[8] G. Vescio, J. Sanchez-Diaz, J. L. Frieiro, R. S. Sánchez, S. Hernández, A. Cirera, I. Mora-Seró, B. Garrido, *ACS Energy Lett* **2022**, *7*, 3653.

[9] L. Liu, D. Zhang, T. Chu, Y. Jian, F. Yu, Y. Wang, Q. Gao, C. Yi, Q. Zhang, L. Sun, Z. Cui, *J Phys D Appl Phys* **2022**, *55*, DOI 10.1088/1361-6463/ac3b0f.

[10] J. Wang, D. Li, Y. Luo, J. Wang, J. Peng, *Adv Mater Technol* **2022**, DOI 10.1002/admt.202200370.

[11] V. R. F. Schröder, N. Fratzscher, F. Mathies, dgar R. Nandayapa, F. Hermerschmidt, va L. Unger, mil J. W. List-Kratochvil, *Nanoscale* **2023**, DOI 10.1039/d3nr00565h.

[12] C.-Y. Huang, S.-P. Chang, A. G. Ansay, Z.-H. Wang, C.-C. Yang, *Coatings* **2020**, *10*, 336.

[13] S. Ahn, K. Yabumoto, Y. Jeong, K. Akagi, *Polym. Chem.* **2014**, *5*, 6977.

[14] J.-H. Lee, S.-H. Cheng, S.-J. Yoo, H. Shin, J.-H. Chang, C.-I. Wu, K.-T. Wong, J.-J. Kim, *Adv Funct Mater* **2015**, *25*, 361.

[15] A. Turak, *Electronic Materials* **2021**, *2*, 198.

[16] F. Hermerschmidt, F. Mathies, V. R. F. Schröder, C. Rehermann, N. Z. Morales, E. L. Unger, E. J. W. List-Kratochvil, *Mater Horiz* **2020**, *7*, 1773.

[17] X. Zhang, H. Lin, H. Huang, C. Reckmeier, Y. Zhang, W. C. H. Choy, A. L. Rogach, *Nano Lett* **2016**, *16*, 1415.

[18] J. Li, L. Xu, T. Wang, J. Song, J. Chen, J. Xue, Y. Dong, B. Cai, Q. Shan, B. Han, H. Zeng, *Advanced Materials* **2017**, *29*, 1603885.

[19] T. Chiba, K. Hoshi, Y.-J. Pu, Y. Takeda, Y. Hayashi, S. Ohisa, S. Kawata, J. Kido, *ACS Appl Mater Interfaces* **2017**, *9*, 18054.